NUCL SCI TECH (2018) 29:89
https://doi.org/10.1007/s41365-018-0416-y

The IH-RFQ for HIRFL-CSR injector

Zhong-Shan Li[1,2] · Xue-Jun Yin[1] · Heng Du[1] · Jia-Wen Xia[1] · You-Jin Yuan[1] · Jian-Cheng Yang[1] · Peng Li[1] · Jie Li[1] · Xiao-Ni Li[1] · Guo-Dong Shen[1] · Wen-Wen Ge[1,2] · Wen-Heng Zheng[1] · Xiao-Hu Zhang[1] · Ke-Dong Wang[1,2] · Yun-Zhe Gao[1,2] · Qi-Yu Kong[1,2]

Received: 7 September 2017 / Revised: 27 November 2017 / Accepted: 2 December 2017 / Published online: 9 May 2018

Abstract A new linac injector CSR-LINAC for the Cooler Storage Ring of the Heavy Ion Research Facility in Lanzhou (HIRFL-CSR) is proposed to improve the performance of the HIRFL. As a key component of the CSR-LINAC, the 108.48-MHz radio frequency quadrupole (RFQ) is under design at the Institute of Modern Physics. Heavy ions with mass-to-charge ratios of 3–7 will be accelerated from 4 to 300 keV/u by the RFQ. In the beam dynamics design, the New Four-Section Procedure is adopted to improve the transmission efficiency and obtain a compact structure. In this paper, a transmission efficiency of 98.0% in the 3.07-m-long cavity was obtained. The Interdigital H-type structure is employed because of its mechanical stability and high shunt impedance. The RF performance of the cavity is investigated by the electromagnetic simulation. The optimized results of the electric field to meet the beam dynamics requirements are presented in this paper.

Keywords Heavy ion linac · Radio frequency quadrupole accelerator · Electromagnetic simulation · Field optimization

This work was supported by the National Natural Science Foundation of China (Nos. 11375243, 11405237, and 11475235) and the Guangdong Innovative and Entrepreneurial Research Team Program (No. 2016ZT06G373).

✉ Xue-Jun Yin
yinxj@impcas.ac.cn

✉ Heng Du
duheng@impcas.ac.cn

1 Institute of Modern Physics, Chinese Academy of Sciences, Lanzhou 730000, China

2 University of Chinese Academy of Sciences, Beijing 100049, China

1 Introduction

To achieve excellent performance in the research of nuclear and atomic physics, the Heavy Ion Research Facility in Lanzhou (HIRFL) was upgraded with a multi-functional Cooler Storage Ring (CSR) at the end of 2007 [1]. As the only injector of the CSR, the Sector Focusing Cyclotron (SFC) is still required to provide ion beams for downstream experiment terminals and the Separated Sector Cyclotron (SSC). The CSR has to be shut down when the SFC provides the beams to experiment terminals or the SSC, which results in the low utilization of the CSR. Furthermore, the SFC has served for nearly 60 years, and it cannot fulfill new experimental requirements, such as the beam current. To solve these problems, a room-temperature heavy ion linac called CSR-LINAC is proposed as a new injector of the CSR to replace the SFC [2], as shown in Fig. 1. The CSR-LINAC consists of a superconducting high charge state Electron Cyclotron Resonance (ECR) Ion Source, a normal-conducting IH-RFQ, and six Interdigital H-type Drift Tube linac (IH-DTL) cavities [3].

Since its invention by Kapchinsky and Teplyakov [4] in the last century, the RFQ accelerator has become an essential part of the hadron accelerators in low-energy section [5, 6] due to its high efficiency. In the recent decades, several RFQs have been designed and constructed for heavy high charge state ion beams, for example the HLI-RFQ at GSI, which accelerates high charge state U^{28+} ions with a duty factor of 50% [7, 8], the SSC-LINAC RFQ of

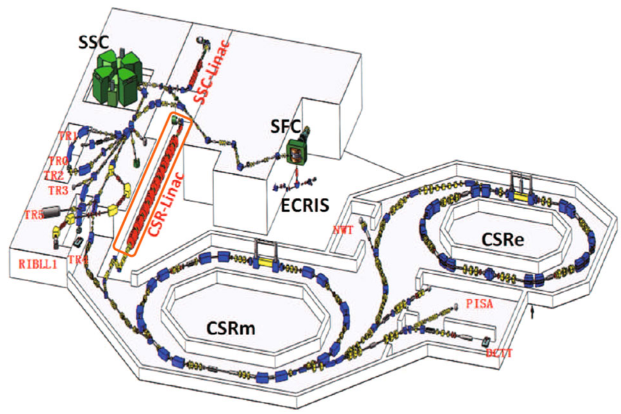

Fig. 1 (Color online) Layout of the HIRFL-CSR with CSR-LINAC

IMP, which is a continuous-wave (CW) mode accelerator for accelerating ions [9, 10], and the MAFF IH-RFQ, which is a pulsed accelerator with a duty factor of 10% that can accelerate ions with mass-to-charge ratios up to 6.3 [11, 12]. The proposed CSR-LINAC RFQ can accelerate 3 emA $^{238}U^{34+}$ beams to 300 keV/u. The maximum duty factor is 0.4% so that this RFQ can be cooled easily. In this paper, the NFSP strategy is adopted to improve the transmission and shorten the cavity length. An error analysis is completed for verifying the error tolerance of the RFQ. The IH-RFQ cavity is employed to achieve excellent RF performance.

2 Beam dynamics

Being upstream of the IH-DTL, the RFQ accelerator supplies the function of changing the initial DC beam to suitable bunches at the desired energy for the requirement of the DTL. The beam dynamics design is based on $^{238}U^{34+}$ beams with current of 3.0 emA and transverse emittance of 0.15 mm·mrad (normalized RMS), which is carried out by the code RFQGen [13]. Some important parameters, such as the operating frequency and inter-vane voltage V must be determined at the first step.

For an RFQ, a higher operating frequency is useful for designing a compact cavity. On the other hand, a lower frequency signifies a larger beam acceptance of the RFQ channel, a better transmission performance, and freer selection of structure parameters [2]. 108.48 MHz is set as the operating frequency of CSR-LINAC RFQ.

The RFQ inputs kinetic energy, at 4 keV/u, and is chosen since the corresponding ECRIS extraction voltage is in an acceptable range of 12–28 kV for the stability and reliability of ECRIS. To ensure the machinability and operation stability of the DTL, the DTL beginning cell length should be longer than 20 mm. Then, the output energy of the RFQ can be designed to be 300 keV/u, which will lead length of the shortest DTL cell of 35 mm. The inter-vane voltage of 68.8 kV is used for the compact RFQ structure and to reduce the risk of RF sparking. The corresponding Kilpatrick coefficient is 2.

The Four-Section Procedure (FSP) [14] developed by Los Alamos National Laboratory (LANL) is a conventional design strategy, which divides a RFQ into four sections: a radial-matcher (RM) section to adapt the time-independent input beam to the time structure of the focusing system, a shaper (SH) section for pre-bunching, a gentle-buncher (GB) section to help change the input beam to proper, small bunches, and an accelerator (ACC) section for a fast energy gain. As the essence of this design method, the GB section keeps the zero current longitudinal phase advance, σ_{0L}, and the geometric length of the separatrix, Z_ψ, constant, which can provide excellent control of the emittance growth induced by the space charge. The σ_{0L} and Z_ψ are determined by the following formulas:

$$\sigma_{0L}^2 = \frac{\pi^2 qeA_{10}V\sin\phi_s}{2Mm_0c^2\beta^2}, \tag{1}$$

$$Z_\psi = \frac{\psi\beta\lambda}{2\pi}, \tag{2}$$

where A_{10} is the acceleration efficiency, V is the inter-vane voltage, ϕ_s is the synchronous phase, M / q is the mass-to-charge ratio, m_0 is the rest mass per nucleon, β is the velocity divided by the speed of light, and ψ is the angular width, which is related to the synchronous phase by $\tan\phi_s = (\sin\psi - \psi)/(1-\cos\psi)$.

However, there are remarkable disadvantages: the synchronous phase ϕ_s and the acceleration coefficient A_{10} rise slowly in the GB section, which results in a long cavity, and the unsmooth evolution of the phase advance leads to beam mismatch and even particle losses. To improve the beam transmission and obtain one compact cavity for the CSR-LINAC RFQ, an unconventional design approach, the New Four-Section Procedure (NFSP) [2, 15, 16] has been employed. The NFSP strategy carefully considers the match between the beam size and the acceleration channel. The transverse focusing factor, B, is varied along with the RFQ to balance the transverse defocusing effect and avoid the parametric resonance [17], especially the case of $\sigma_{0T} < \sigma_{0L}$ in the traditional FSP (see Fig. 2c). σ_{0T} and B are given by:

$$\sigma_{0T}^2 = \frac{B^2}{8\pi^2} - \frac{\sigma_{0L}^2}{2}, \tag{3}$$

$$B = \frac{qeV\lambda^2 X}{Mm_0c^2a^2}, \tag{4}$$

where λ is the RF wavelength, a is the minimum aperture radius, and X is focusing efficiency. The non-resonant

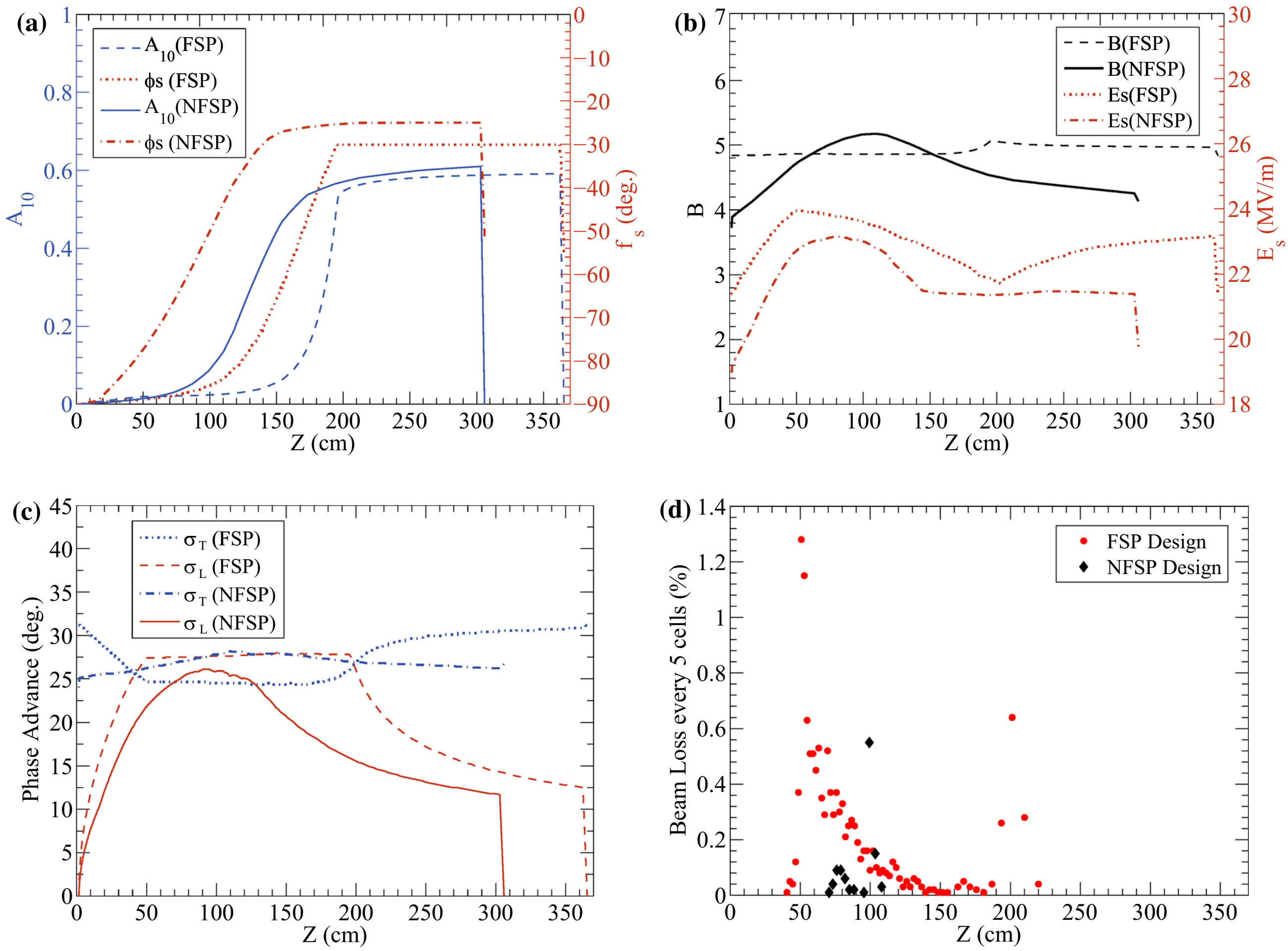

Fig. 2 (Color online) The comparisons of beam dynamics of the FSP and NFSP designs

stable region requires $B > 2\sqrt{3}\pi\sigma_{0L}$. In the new SH section, the parameter B increases gradually as the transverse defocusing factor due to the growing acceleration coefficient A_{10}. The ascending B in the SH section and the variable Z_ψ allow ϕ_s and A_{10} to rise much more rapidly than in the original GB section. In the ACC section, B should decrease since the transverse defocusing factor is reduced because of the rapidly increasing beam energy.

The comparisons of beam dynamics between the FSP and NFSP designs of CSR-LINAC RFQ are shown in Fig. 2. As shown in Fig. 2a, ϕ_s and A_{10} in the NFSP GB section increase much more rapidly than in the FSP GB section, and the cavity length of the NFSP design is 58 cm shorter than the FSP design. Figure 2b shows the comparison of the transverse focusing factor, B, and peak electric field, E_s, in the FSP and NFSP design. The maximum value of B in the NFSP design is larger than in the FSP design, while the maximum value of E_s in the NFSP design is smaller. In the FSP GB section, the σ_{0L} is larger than σ_{0T} (the dash curves in Fig. 2c), which causes parametric resonance and significant particle losses in the transverse plane (the red dots in Fig. 2d). The solid curves shown in Fig. 2c represent σ_{0T} and σ_{0L} in the NFSP design, which shows that the curves of σ_{0T} and σ_{0L} have been separated. Beam losses are also diminished, as shown in Fig. 2d (the black dots).

Figure 3 shows the beam transmission along the RFQ. Particle losses occur mainly at the end of the GB section (around the 177th cell) and the ACC section (around the 225th cell). For $^{238}U^{34+}$ beams with a current of 3 emA, the transmission efficiency of 98.0% is reached. Figure 4 shows the beam phase space projection at the entrance and exit of RFQ. The FWHM energy spread is about 2.4% at the exit of the RFQ. The main parameters of the CSR-LINAC RFQ are listed in Table 1.

3 Error analysis

In actual operation, the beam parameters at the entrance of the RFQ and the inter-vane voltage have some differences with the design values, which may significantly

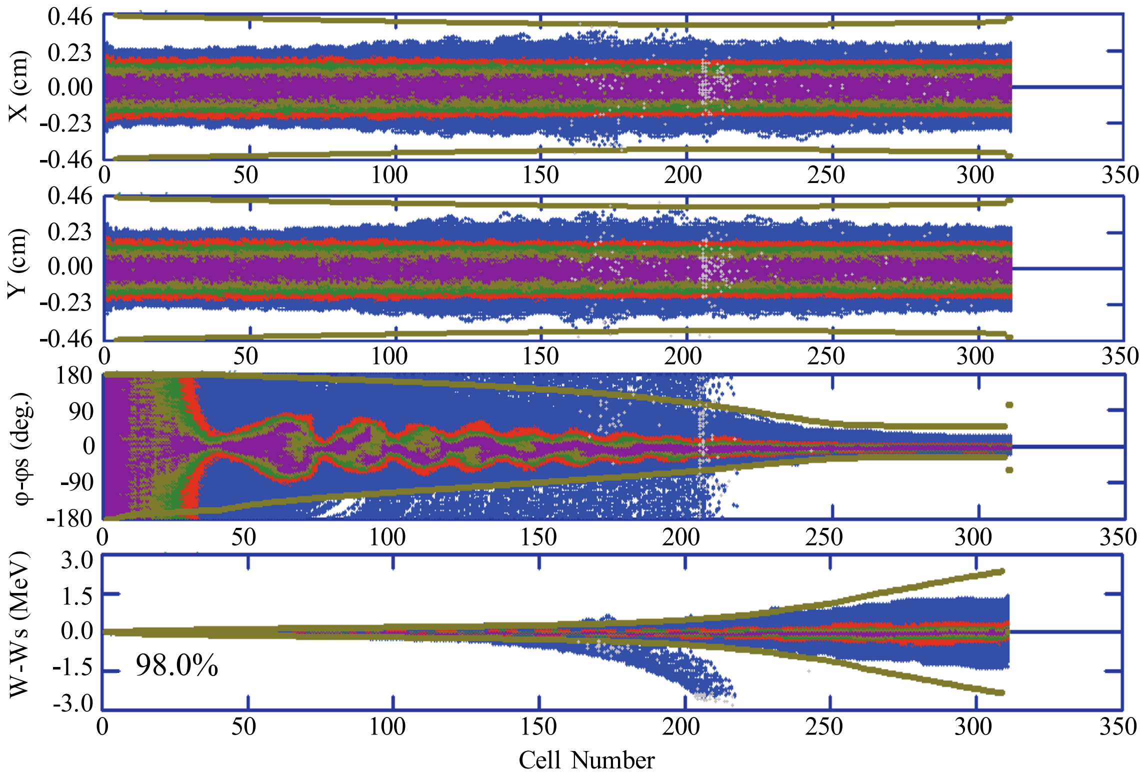

Fig. 3 (Color online) Beam transmission along the RFQ. Plots from top to bottom are the beam profiles in the horizontal and vertical planes, the phase, and the energy spectra, respectively

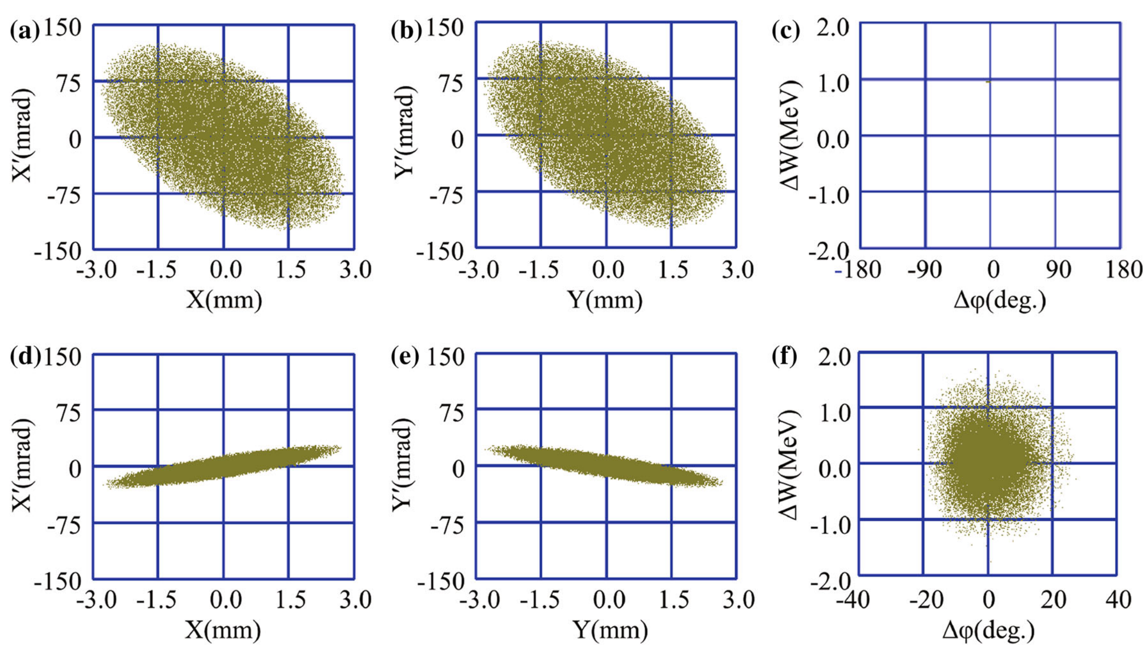

Fig. 4 (Color online) The beam phase space projection at the entrance and exit of the RFQ. **a**–**c** are the horizontal, vertical, and longitudinal phase space at the entrance, respectively; **d**–**f** are the horizontal, vertical, and longitudinal phase space at the exit, respectively

influence the beam transmission in the RFQ channel. Hence, it is valuable to analyze the impact on the RFQ sensitivity and stability caused by non-ideal input beams and vane voltage deviation. The design values of the beam parameters at the entrance of the RFQ are the beam transverse emittance $\epsilon = 0.15$ mm·mrad (normalized

Table 1 Parameters of the beam dynamics design

Parameters	Values
Frequency (MHz)	108.48
Mass-to-charge ratios	3–7
Beam current ($^{238}U^{34+}$) (emA)	3.0
Input energy (keV/u)	4
Output energy (keV/u)	300
Inter-vane voltage (kV)	68.8
Kilpatrick coefficient	2.0
Minimum aperture (mm)	2.63
Modulation	1.0–2.124
Synchronous phase (°)	− 90 to − 25
Input transverse emittance (normalized RMS) (mm·mrad)	0.15
Output transverse emittance (normalized RMS) (mm·mrad)	0.149
Length of the cavity (cm)	307
Transmission efficiency (3 emA $^{238}U^{34+}$) (%)	98.0

RMS), $\alpha = 0.6$, $\beta = 2.6$ cm/rad, the beam current of 3 emA, and the energy of 4 keV/u with zero energy spread and 360° phase width. The design inter-vane voltage is 68.8 kV. One parameter was changed, and others were kept constant during the error analysis. In Fig. 5, the current changes from 0 to 20 emA, and the efficiency remains relatively high for values less than 7.0 emA. As such, this design leaves a large margin for future updates and extensions. Figure 6 presents that the input beam energy deviation has an effect on the transmission efficiency. The transmission slowly declines when the absolute value of the input energy deviation is less than 3%. Figure 7 shows that, for the design Twiss parameters, a large emittance, which means a large beam size, induces a transmission decay, and a lower emittance causes transmission efficiency decreases as well because it enhances the space charge effect due to the smaller beam size. Figure 8 shows

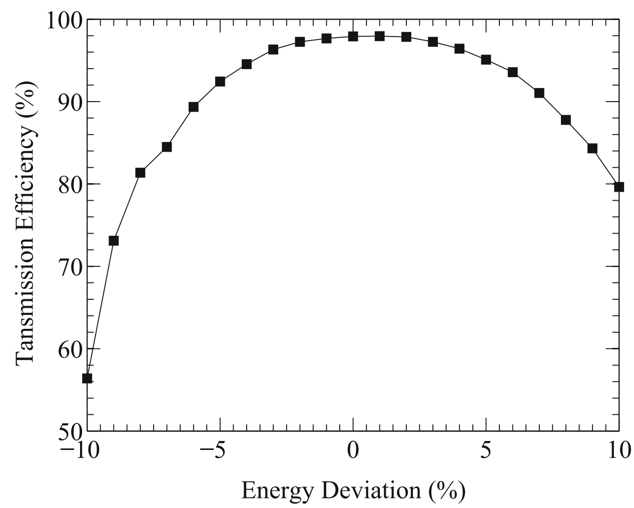

Fig. 6 Transmission efficiency versus input energy deviation

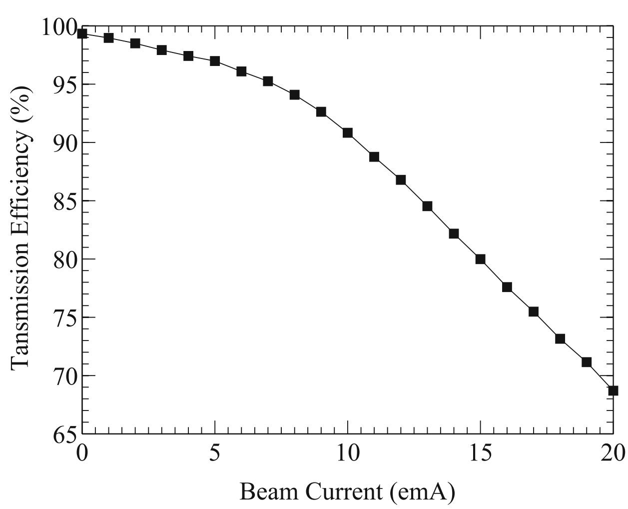

Fig. 5 Transmission efficiency versus input beam current

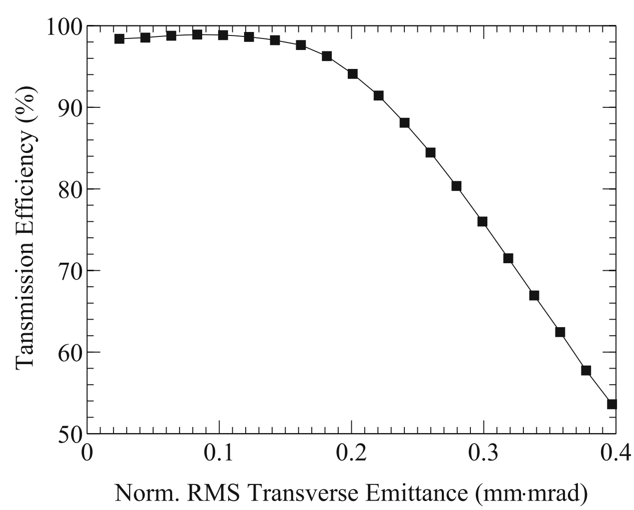

Fig. 7 Transmission efficiency versus input emittance

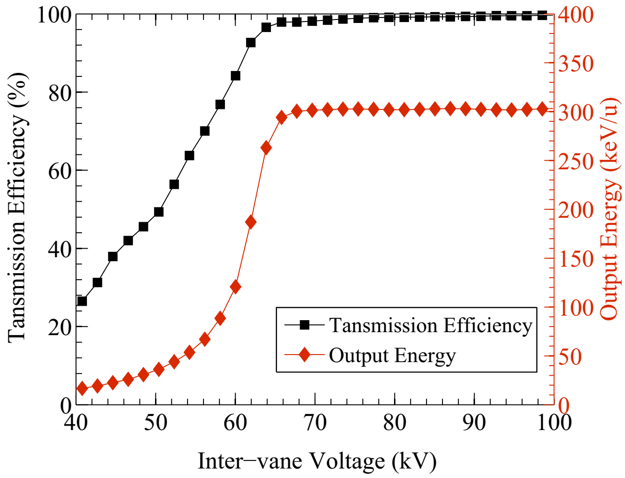

Fig. 8 Transmission efficiency and output energy versus inter-vane voltage

the plots of the transmission efficiency and output energy versus inter-vane voltage. To meet the design requirements of transmission and output energy, the inter-vane voltage must be more than 67 kV. Figure 9 shows the contour map of the transmission efficiency and transverse emittance growth for different input Twiss parameters. The white point in the figure represents the design value. Figures 10 and 11 show contour maps of the transmission efficiency and transverse emittance growth with input beam center and beam center angle offset, respectively. To get high transmission efficiency and the emittance growth to be less than 10%, the input beam center and beam center angle offset must be in the range of ± 0.4 mm and ± 20 mrad, respectively.

4 RF design

The CST Microwave Studio (MWS) [18] code was used for the RF design of the CSR-LINAC RFQ with respect to resonance frequency, field distribution, and power losses. The impact of the non-ideal field distribution on the beam dynamics is investigated by the TraceWin [19] code.

The IH-type RF structure was chosen since this structure was demonstrated to have a higher shunt impedance and mechanical stability [20, 21]. Figure 12 shows the CST model of the IH-RFQ, which consists of a cylinder, 4 mini-vane rods, 31 stems, and 2 supporter plates. There is strong RF coupling along the cavity by the longitudinal magnetic field, which leads to a homogeneous distribution of wall losses. The overall power loss in the cavity walls is comparatively small, which results in a high shunt impedance. The electrical conductivity of the copper was set to 5.0×10^7 S in the electromagnetic simulation based on the consideration of RF contact resistance in the installation

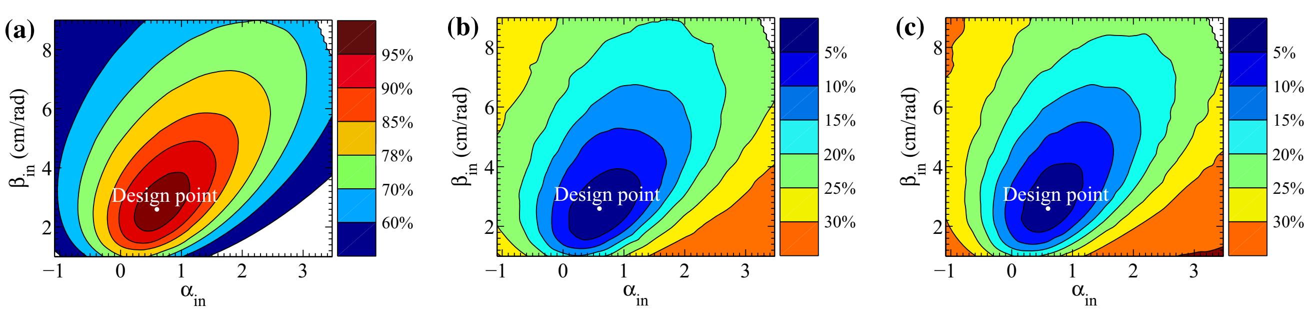

Fig. 9 (Color online) Transmission efficiency (**a**), horizontal emittance growth (**b**), and vertical emittance growth (**c**) versus input beam Twiss parameters

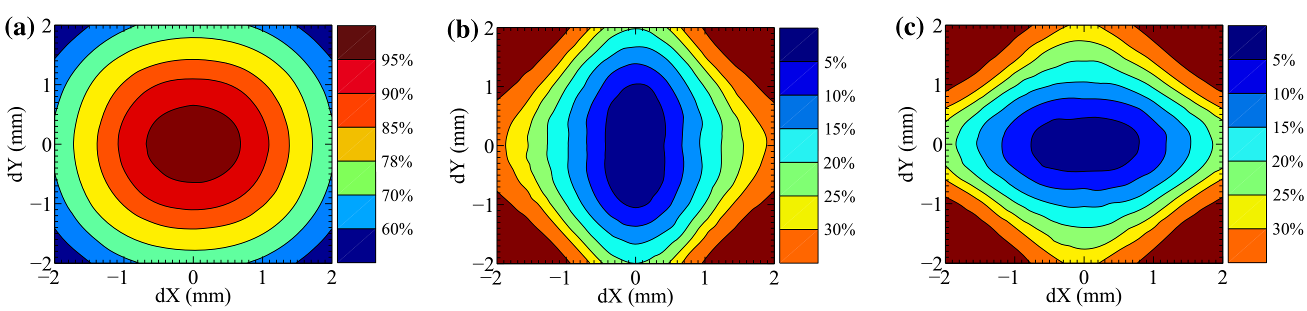

Fig. 10 (Color online) Transmission efficiency (**a**), horizontal emittance growth (**b**), and vertical emittance growth (**c**) versus beam center offset at the entrance

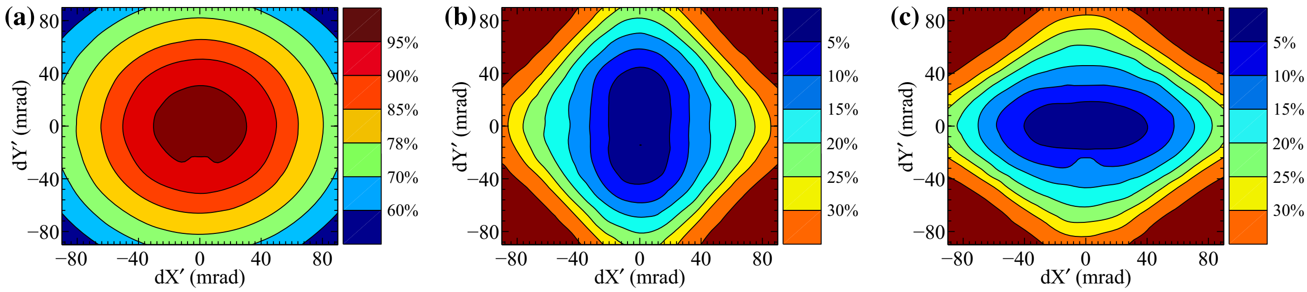

Fig. 11 (Color online) Transmission efficiency (**a**), horizontal emittance growth (**b**), and vertical emittance growth (**c**) versus beam angle offset at the entrance

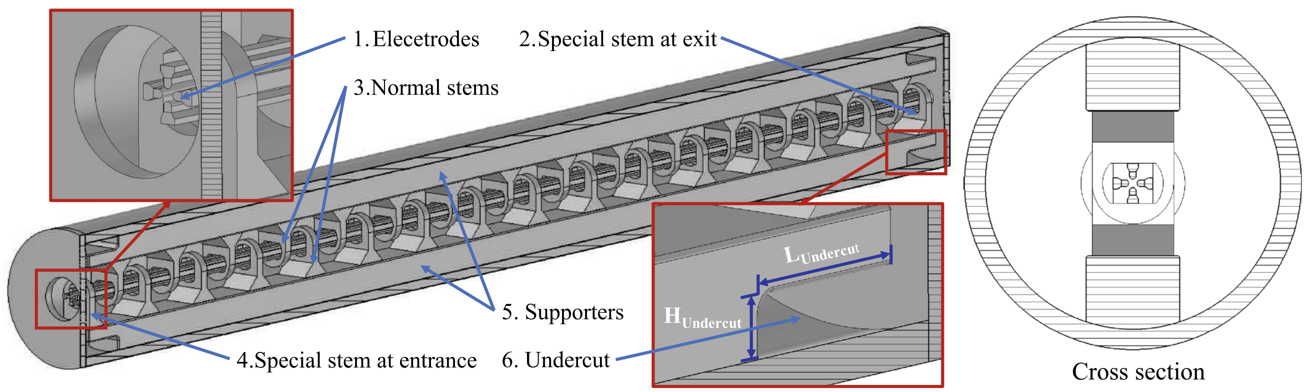

Fig. 12 The CST model of the IH-RFQ

Table 2 The main RF parameters of the CSR-LINAC RFQ

RF parameters	CST simulation values
Frequency (MHz)	108.15
Q_0	5910
Power loss (kW)	123
R_s (kΩm)	118

plane. The RF parameters, simulated by the MWS code, are presented in Table 2. The RF power of 123 kW is needed to accelerate $^{238}U^{34+}$ beams to the design energy, and then, a 200-kW RF transmitter with some margin is required for the RF power supply.

The beam dynamics design requires a flat inter-vane voltage distribution. However, in practice the field is different from the dynamics requirement, which can be described as the quadrupole field unflatness and the dipole field. The quadrupole field unflatness is mainly caused by non-uniform capacitive loading along the whole cavity and stray capacitances between the wall and the rods. It can be calculated with the following formula:

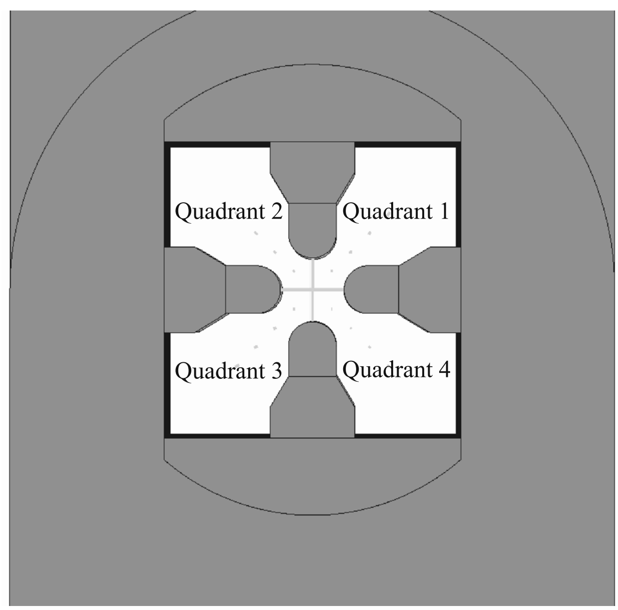

Fig. 13 The number of each quadrant. This figure shows the view from the entrance of the cavity

$$\text{Unflatness} = \frac{V - \bar{V}}{\bar{V}}, \tag{5}$$

where $\bar{V}$ is the average value of V; $V = (V_1 + V_2 + V_3 + V_4)/4$; and V_1, V_2, V_3, and V_4 are inter-vane voltages of the 1st, 2nd, 3rd, and 4th quadrants, respectively. Each quadrant in the RFQ is shown in Fig. 13. The dipole field is caused by the asymmetry of the RF structure, which can be represented by:

$$\text{Dipole} = \frac{V_1 + V_2 - V_3 - V_4}{V}. \tag{6}$$

Figure 14a shows that the quadrupole field unflatness is between -21 and 12% in the preliminary RF design, which is not satisfied for the beam transmission. Furthermore, the beam dynamics simulation with this unflatness indicates that it can cause an additional energy deviation at the RFQ exit. This result does not meet the requirement of the DTL structure. At the same time, the quadrupole field unflatness changes the Kilpatrick coefficient from 2 to 2.24 when leads to the increased risk of RF sparking. To the optimization of the quadrupole field unflatness, the tuning method of the magnetic flux induction by variation of the girder that undercuts lengths at both tank ends is applied, as shown in Fig. 12. Figure 14b shows the quadrupole field unflatnesses after optimizing. When the height of undercuts is 40 mm, the lengths of the undercut at the entrance and exit are 120 mm and 170 mm, respectively, and the

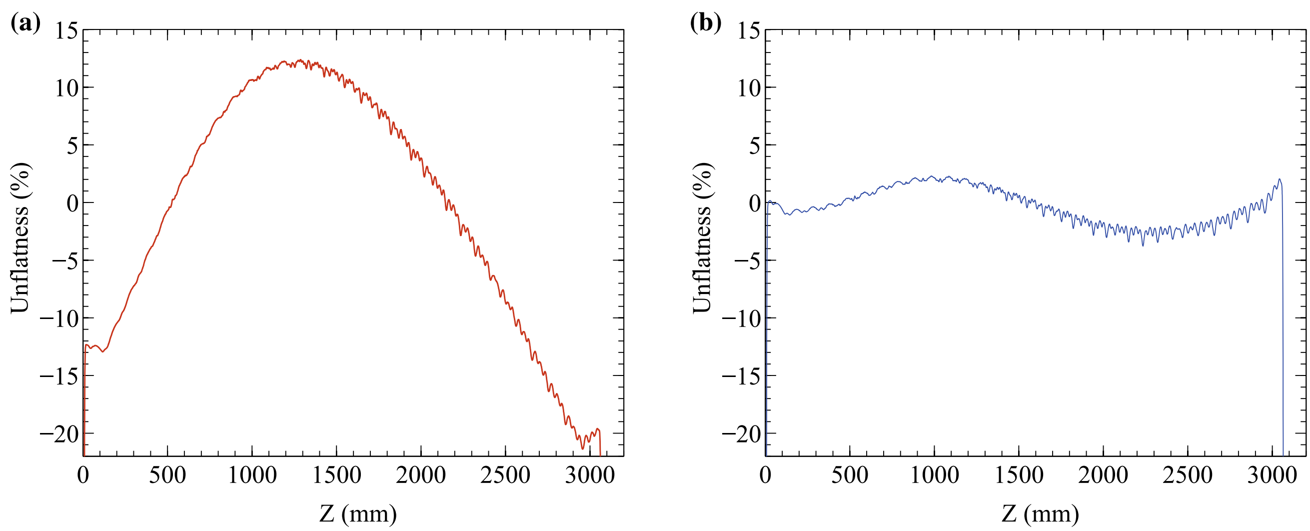

Fig. 14 The quadrupole field unflatness optimization. Plots from left to right are the quadrupole field unflatness distribution before and after optimizing, respectively

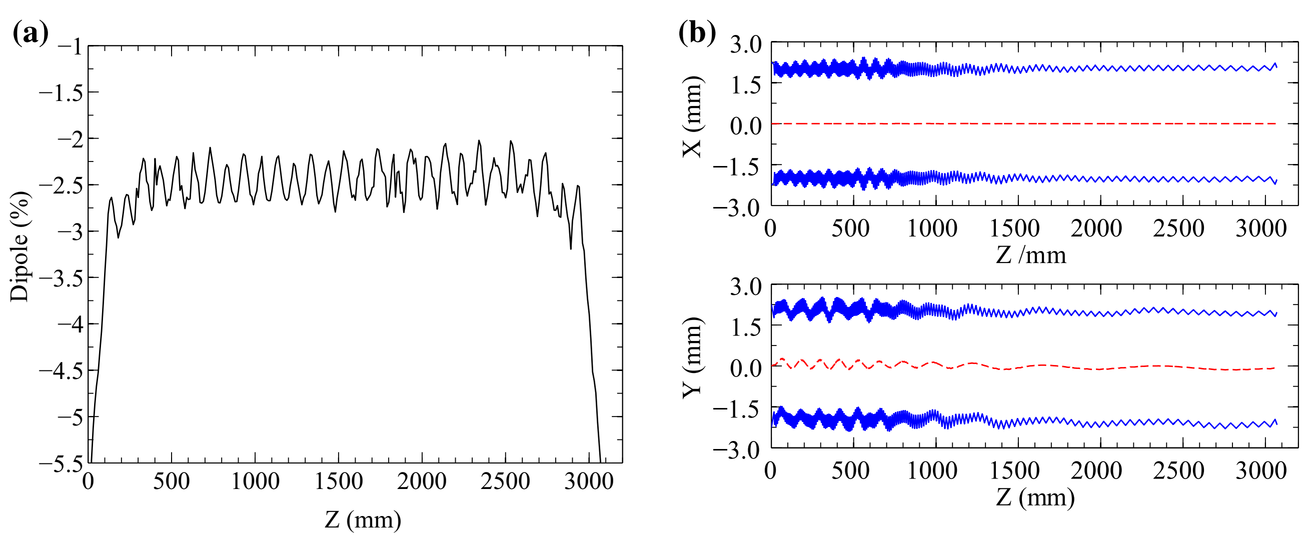

Fig. 15 The dipole field and its effect. The left figure is the distribution of the dipole field, and the right is the distribution of beam envelope and center with dipole field. The solid line is the beam envelope, and the dash line is the beam center

quadrupole field unflatness is at a minimum ($\pm 2.5\%$), which then has no effect on the output energy.

The dipole field will cause the oscillation of the beam center. Figure 15a shows that the distribution of the dipole field along the RFQ ranges from -3.2 to -2.1%. The beam dynamics simulation results show that the dipole field of $-3.2\sim-2.1\%$ causes a slight oscillation of the beam center, as shown in Fig. 15b. The transmission efficiency is still 98.0%. This means that the dipole field does not need to be decreased any more.

5 Conclusion

The beam dynamics study and RF design of an IH-RFQ for CSR-LINAC are finished at the Institute of Modern Physics. This RFQ accelerates heavy ion $^{238}U^{34+}$ beams with a current of 3.0 emA from 4 to 300 keV/u. The NFSP design method was applied to achieve the transmission efficiency of 98.0% with a 3.07-m-long cavity. The transmission of the $^{238}U^{34+}$ beams for different input beam parameters and inter-vane voltages was investigated. The simulation results show that this beam dynamics design has a wide compatible margin for non-ideal beams. The RF performance of the IH-RFQ was simulated by the CST MWS code. The RF power for the acceleration of $^{238}U^{34+}$ beams is 123 kW. The quadrupole field unflatness of $\pm 2.5\%$ and the dipole field of $-3.2\sim-2.1\%$ were obtained, which have little effect on the beam transmission.

References

1. J.W. Xia, W.L. Zhan, B.W. Wei et al., The heavy ion cooler-storage-ring project (HIRFL-CSR) at Lanzhou. Nucl. Instrum. Meth. A **488**, 11 (2002). https://doi.org/10.1016/s0168-9002(02)00475-8
2. X.H. Zhang, Y.J. Yuan, J.W. Xia et al., Conceptional design of a heavy ion linac injector for HIRFL-CSRm. Chin. Phys. C **38**, 10 (2014). https://doi.org/10.1088/1674-1137/38/10/107002
3. X.H. Zhang, H. Du, J.W. Xia, et al., THPWO059: beam dynamics design of the main accelerating section with KONUS in the CSR-LINAC proposal, in *The 4th International Particle Accelerator Conference (IPAC2013)*, Shanghai, China. May 12–17 (2013)
4. I.M. Kapchinskii, V.A. Teplyakov, Linear ion accelerator with spatially homogeneous strong focusing. Pribory i Teknika Eksperimenta **23**, 19–22 (1969)
5. B. Mustapha, A.A. Kolomiets, P.N. Ostroumov, Full three-dimensional approach to the design and simulation of a radio-frequency quadrupole. Phys. Rev. ST Accel. Beams **16**, 120101 (2013). https://doi.org/10.1103/PhysRevSTAB.16.120101
6. T.P. Wangler, Principles of RF linear accelerators, in T.P. Wangler, ed. (Wiley, Berlin, 2008), pp. 232–281
7. J. Friedrich, A. Schempp, H. Deitinghoff, et al., Properties of the GSI HLI-RFQ structure, in *The 1991 IEEE Particle Accelerator Conference (PAC1991)*, San Francisco, California, USA, May 6–9 (1991)
8. J. Friedrich, A. Schempp, H. Deitinghoff, et al., Performance of the GSI HLI-RFQ, in *The Third European Particle Accelerator Conference (EPAC1992)*, Berlin, Germany, March 24–28 (1992)
9. G. Liu, Y.R. Lu, Y. He et al., Design of a CW high charge state heavy ion RFQ for SSC-LINAC. Nucl. Instrum. Meth. A **701**, 3 (2013). https://doi.org/10.1016/j.nima.2012.11.017
10. X.J. Yin, Y.J. Yuan, J.W. Xia et al., Design, fabrication, and beam commissioning of a continuous-wave four-rod rf quadrupole. Phys. Rev. ST-Accel. Beams **19**, 010402 (2016). https://doi.org/10.1103/PhysRevAccelBeams.19.010402
11. M. Pasini, O. Kester, D. Habs, et al., TUPLT034: beam dynamics studies for the low energy section at MAFF, in *The Nineth European Particle Accelerator Conference (EPAC2004)*, Lucerne, Switzerland, July 5–9 (2004)
12. H. Zimmermann, A. Bechtold, D. Habs, et al., MOPP111: Beam tests with the MAFF IH-RFQ at the IAP-FRANKFURT, in *The 11th European Particle Accelerator Conference (EPAC2008)*, Genoa, Italy, June 23–27 (2008)
13. L. Young, *RFQGen User Guide* (Los Alamos Scientific Lab, Los Alamos, NM, 2016)
14. K.R. Crandall, S4-1: RF quadrupole beam dynamics design studies, in *The 1979 Linear Accelerator Conference*, Montauk, New York, USA, September 10–14 (1979)
15. X.H. Zhang, Beam dynamics design and research of the linac injectors in HIRFL. Ph.D. Thesis, University of Chinese Academy of Sciences (2014)
16. C. Zhang, A. Schempp, Beam dynamics studies on a 200mA proton radio frequency quadrupole accelerator. Nucl. Instrum. Meth. A **586**, 2 (2008). https://doi.org/10.1016/j.nima.2007.12.001
17. I.M. Kapchinsky, Selected topics in ion linac theory, Lecture given at the University of Maryland (1993)
18. Computer Simulation Technology (CST), Micro Wave Studio. https://www.cst.com/
19. D. Uriot, N. Pichoff, TraceWin documentation. http://irfu.cea.fr/Sacm/logiciels/index3.php
20. U. Ratzinger, K. Kaspar, E. Malwitz et al., TUPLT033: The GSI 36 MHz high-current IH-type RFQ and HIIF-relevant extensions. Nucl. Instrum. Meth. A **415**, 1 (1998). https://doi.org/10.1016/S0168-9002(98)00395-7
21. M. Pasini, T. Sieber, D. Habs, et al., RF design of the MAFF IH-RFQ power resonator, in *The ninth European Particle Accelerator Conference (EPAC2004)*, Lucerne, Switzerland, July 5–9 (2004)